

## Dual-Functional Orthopedic Implants Based on $\text{Al}_2\text{O}_3$ - $\text{CuO}$ /Ti NanoComposite: Antimicrobial and Osteogenic Properties

H. Bayat<sup>1</sup>, P. Sangpour<sup>1</sup>, M. Heydari<sup>1,\*</sup>, L. Nikzad<sup>2</sup>

\* [m.heydari@merc.ac.ir](mailto:m.heydari@merc.ac.ir)

<sup>1</sup> Department of Nano Technology and Advanced Materials, Materials and Energy Research Center, Karaj, Iran

<sup>2</sup> Department of Ceramic, Materials and Energy Research Center, Karaj, Iran

Received: July 2025

Revised: November 2025

Accepted: December 2025

DOI: [10.22068/ijmse.4180](https://doi.org/10.22068/ijmse.4180)

**Abstract:** In this study, we investigated the antimicrobial, bioactivity, and *in vitro* cytotoxicity of a nanocomposite made of copper oxide ( $\text{CuO}$ ) and aluminum oxide ( $\text{Al}_2\text{O}_3$ ) with two different morphologies of copper oxide (Spherical- $s\text{CuO}$  and Nanoplate- $p\text{CuO}$ ), which was made using the Spark Plasma Sintering (SPS) process on a titanium substrate as an orthopedic implant. Two different weight percents of copper oxide nanostructures of  $s\text{CuO}$  NP (10 wt%, 20 wt%) and  $p\text{CuO}$  NP (10 wt%, 20 wt%) have been used in this research. Synthesized nanocomposites were investigated by X-ray diffraction (XRD), X-ray photoelectron spectroscopy (XPS), Fourier transform infrared spectroscopy (FTIR), and field emission scanning electron microscope (FESEM). Based on the obtained results, the XRD pattern and XPS confirmed that the nanocomposites were successfully synthesized without impurity. FESEM images revealed that  $\text{CuO}$  nanoparticles and nanoplates were distributed uniformly on the alumina matrix. The antibacterial activity of the synthesized nanocomposites was investigated using *Escherichia coli* (*E. coli*) and *Staphylococcus aureus* (*S. aureus*), two bacteria, one gram-negative and the other gram-positive. Antibacterial activity results showed that  $\text{CuO}$  nanoparticles had high antibacterial activity, and the effect of  $\text{CuO}$  nanostructures depended not only on their morphology and size, but also on the type of microorganisms. Furthermore nanocomposite with nanoplate copper oxide exhibited more bioactivity properties than the spherical shape. *S. aureus* showed greater resistance to  $\text{CuO}$  nanostructure, while *E. coli* was more susceptible to them (15%). In addition, toxicity tests showed that nanoplate copper oxide exhibited greater toxicity due to its high surface reactivity than spherical nanoparticles. This study provides new insights into the role of copper oxide nanoparticle morphology in the properties of nanocomposites for use as orthopedic implants.

**Keywords:** Nanocomposite,  $\text{CuO}$ , Alumina, SPS, Antibacterial properties.

### 1. INTRODUCTION

Titanium and its numerous alloys are widely used in the area of orthopedic implants due to their outstanding mechanical characteristics, ability to resist corrosion, and their biocompatibility [1]. Ti and Ti alloys still lack in their antibacterial capabilities and ability to promote bone growth. Therefore, further research and development are needed to improve their performance in these areas [2].

Despite the considerable advancements in healthcare, the risk of contracting an infection during surgical procedures continues to be substantial, with a worldwide infection risk of 1-2% in orthopedic surgeries [3]. Device infections can progress when bacteria adhere to implants and form biofilms, shielding them from the immune system. Exposing titanium to air results in the formation of a thin layer of titania on its surface, rendering it suitable for use as a bio inert material. This entails costly and intricate clinical interventions, posing a significant medical challenge that is being addressed

through innovative treatment approaches utilizing nanomaterials and nanocomposites [4].

Nanocomposites combine the advantages of nanomaterials, such as chemical resistance, high conductivity, biocompatibility, and elasticity. Nanocomposites are highly active nanostructures that offer unique combinations and engineering possibilities. Their rapid growth and reactivity in different surfaces make them highly valuable for various biological applications [5], such as antibacterial properties and biocompatibility applications. Recently, several reports have focused on metal oxides such as aluminum oxide ( $\text{Al}_2\text{O}_3$ ), copper oxide ( $\text{CuO}$ ), and nickel oxide ( $\text{NiO}$ ). In addition, increasing emphasis has been placed on the potential of copper oxide in various areas such as antibacterial properties [6, 7].

$\alpha$ ,  $\beta$ , and  $\gamma$ - $\text{Al}_2\text{O}_3$  are common phase modifications of  $\text{Al}_2\text{O}_3$ .  $\alpha$ - $\text{Al}_2\text{O}_3$  is the most occurring form. Aluminum Oxide nanoparticle ( $\text{AlOxNPs}$ ) are of interest for biomedical uses, especially as an antibacterial agent. Limited data exists on their mechanisms for acting on microbial growth [8].

Bacteriostatic effect involves electrostatic interaction with bacterial membrane/cell wall as well as the formation of aluminum cations ( $Al^{3+}$ ) that initiate the generation of Reactive oxygen Species (ROS). The interaction of  $Al^{3+}$  with cell membrane phospholipids causes various structural and functional disorders. These disorders involve direct interaction with proteins, leading to the creation of ion channels, receptors, and enzymes. Additionally,  $Al^{3+}$  induces structural changes in the lipid membrane and affects the activity at the lipid/protein interface [9, 10].

Pakrashi et al. [11] showed a greater antibacterial activity of the  $\alpha$ -phase of aluminum oxide compared to  $\gamma$ -aluminum oxide against *Bacillus licheniformis* after a two-hour exposure to aluminium oxide. This was evident in a higher content of ROS after exposure to  $\alpha$ - $Al_2O_3$  ( $2.6 \pm 0.02\%$ ) compared to  $\gamma$ - $Al_2O_3$  ( $0.6 \pm 0.003\%$ ) at an  $AlOxNP$  concentration of  $5 \mu\text{g/mL}$  [11]. The toxicity of alumina nanoparticles has been studied in the past decades, but due to the physical and chemical complexity and the lack of control in a microcosm, it is difficult to draw definitive conclusions from dynamic studies. Therefore, nanomaterials may not exhibit the expected toxic response at low concentrations over extended periods [12]. Among the various types of metal oxides, Copper oxide (CuO) is a p-type narrow bandgap semiconductor with outstanding electrochemical, catalytic, photocatalytic, and antibacterial properties [13]. CuO nanoparticles have been made with different methods like hydrothermal, solvothermal, thermal oxidation, sonochemical, and microwave irradiation [14]. Efforts focus on creating synthesized CuO nanostructures with various shapes to improve its effectiveness [15]. Like most metal oxides, the primary mechanism for achieving antibacterial activity is the electrostatic interaction of nanoparticles with the bacterial outer membrane/cell wall and the generation of Reactive Oxygen Species (ROS) [16, 17]. Studies show that nanoparticles with different sizes, shapes, compositions, and surface charges have various antibacterial properties due to differences in their ability to generate ROS [18]. Shima Tavakoli et al. demonstrated the impact of morphology on the antibacterial properties of CuO; the microbial sensitivity to CuO-NPs depended on the microbial species and nanoparticle morphology and properties [19].

Different techniques have been introduced to coat the ceramics on a metal implant surface. The Spark

Plasma Sintering (SPS) technique presents itself as a revolutionary method in the realm of advanced material synthesis and coating technologies. Known for its ability to rapidly consolidate nanocomposites, SPS offers distinct advantages over traditional sintering processes, including shorter sintering cycles, lower temperatures, and enhanced material densification [20, 21]. In a research performed by Christophe Tenailleau et al. a copper/zinc oxide nanocomposite was developed using the SPS method. This nanocomposite exhibited high densification within a very brief period of heat treatment under high pressure [22]. So, the application of SPS in this study introduces a dual advantage of antimicrobial efficacy and osteogenic potential. By leveraging SPS's ability to retain nanoparticle morphology and create highly adherent, uniform coatings, the research highlights a promising pathway for developing next-generation orthopedic implants.

In addition, the simultaneous sintering and bonding of copper oxide and alumina resulted in enhanced antibacterial activity and bioactivity due to synergistic interactions between the materials. Such effects are rarely achievable through traditional coating methods. Furthermore, the methodology emphasizes the role of nanocomposite morphology—a topic underexplored in current literature—thereby contributing novel perspectives to the field of biomedical material science.

Therefore, in this study, SPS was employed to deposit CuO- $Al_2O_3$  nanocomposite coatings on titanium substrates, unveiling novel insights into antibacterial and osteogenic properties that are critical for orthopedic applications.

## 2. EXPERIMENTAL PROCEDURES

### 2.1. Materials and Methods

Industrial pure Ti grade II was cut into pieces of  $15 \text{ mm} \times 5 \text{ mm}$ . Ti wafers were base with different sizes of the metallographic sandpaper, polished, and ultrasonically cleaned in ethanol.  $\alpha$ - $Al_2O_3$  and spherical CuO (sCuO-NP) were purchased from US-Research Nanomaterials; the average particle size of the powders was around 150 nm and 50 nm, respectively, Fig. 1(a,c).

### 2.2. Synthesis of CuO Nanoplates

Copper (II) sulfate pentahydrate ( $CuSO_4 \cdot 5H_2O$ ) was purchased from MERCK as precursor for the synthesis of CuO nanoplates (pCuO).

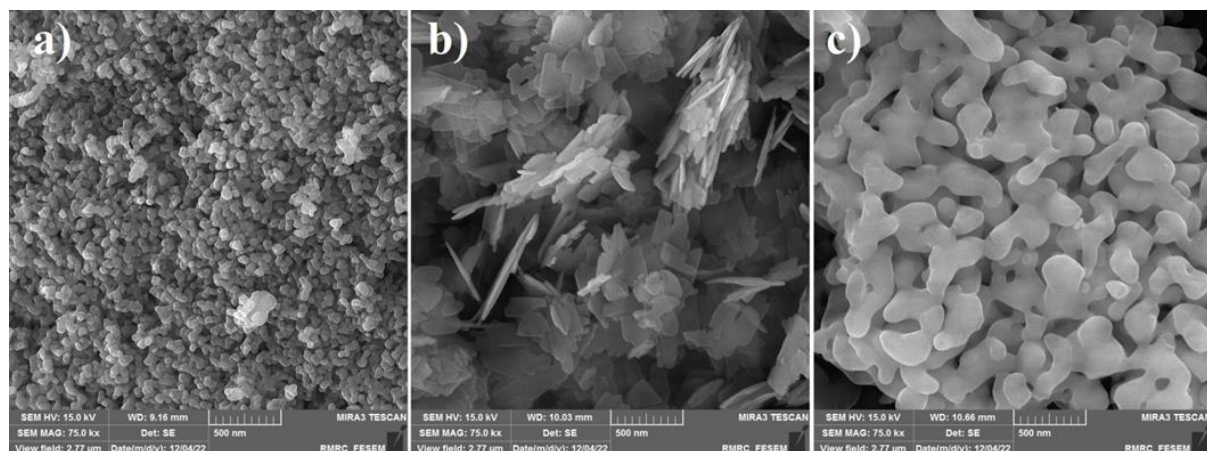


**Fig. 1.** FESEM images of raw material: a) Spherical shape of copper oxide (sCuO), b) homemade synthesized nanoplate of copper oxide (pCuO), and c) Alumina ( $\alpha$ -Al<sub>2</sub>O<sub>3</sub>)

The solution of CuSO<sub>4</sub>·5H<sub>2</sub>O (0.1 M) was prepared in 100 mL of distilled water. The NaOH solution (1 M) was added drop by drop until the pH of the reactants increased to 13. The solution was next transferred into a Teflon-lined sealed stainless steel hydrothermal autoclave and maintained at a constant temperature of 100°C for 18 hours under autogenous pressure. Then it was cooled to room temperature. The sediment then obtained is placed in a furnace and annealed in air at 40°C for 48 hours. Scheme 2 shows a schematic of synthesis of CuO nanoplates.

### 2.3. Deposition of Nanocomposite Thin Films

In order to prepare nanocomposite thin films,  $\alpha$ -Al<sub>2</sub>O<sub>3</sub> powders and CuO nanostructures were mixed using a SPEX (8000D Mixer/Mill, USA) for 15 min with simple horizontal vibrating. Nanocomposites with different weight percentages of sCuO NP (10 wt%, 20 wt%) and pCuO NP

(10 wt%, 20 wt%) were coated on the Ti substrates by using the SPS technique. Table 1 shows the SPS parameters.

**Table 1.** SPS parameters

Current	0.77 A
Vacuum chamber	30 Mpa
Pressure	40 Mpa
Temprature	1000°C

### 2.4. Characterization

Synthesized nanocomposites were characterized using FESEM (MIRA3, TESCAN-XMU, Czech Republic) to investigate morphology, cross-section, and size of NPs. To investigate the elemental composition of the nanocomposite, X-ray diffraction (XRD) was carried out using Philips PW3710 Cu K $\alpha$  (at 45 kV, 30 mA, scanning speed 20 minute<sup>-1</sup>, step size: 0.02, step time: 0.5 s).

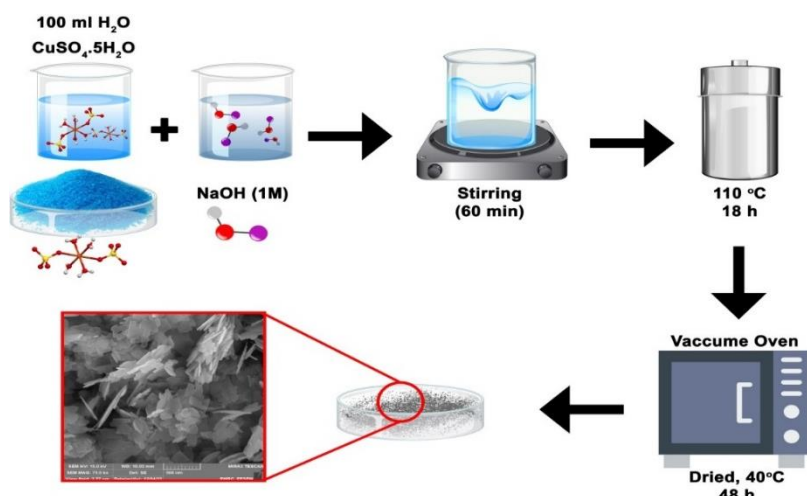


**Fig. 2.** Schematic of the synthesis of CuO nanoplates

The patterns were analyzed using X'Pert High Score software. The X-ray photoelectron spectrometer (XPS-Al K $\alpha$  anode) was used to investigate the chemical bonds present in the nanocomposites. XPS at an energy of 1486.6 eV was employed to investigate the surface atomic composition and chemical state. Fourier transform infrared (FTIR) spectroscopy (LR 64912C, Perkin Elmer) was used to analyze the different functional groups of the adsorbent through the KBr pellet method.

### 2.5. Antibacterial Activity

*Escherichia coli* (E. coli) ATCC 25922 (Gram-negative bacteria) and *Staphylococcus aureus* (S. aureus) ATCC 45500 (Gram-positive bacteria) were utilized for measuring the effect of antibacterial properties of pure and coated titanium by the unit colony formation (CFU) method. E. coli and S. aureus bacteria were initially cultured in Luria-Bertani (LB) agar medium, which consisted of 10 g/L peptone, 5 g/L yeast extract, 5 g/L NaCl, and incubated at 37°C for 18 hours. The suspension was prepared from the freshly grown culture in sterile physiological serum to achieve a concentration of 0.5 Mac Farland ( $1.5 \times 10^8$  cfu/ml), resulting in  $1.5 \times 10^6$  cfu/ml. All samples and controls were incubated in sterile flasks with the suspension at 37°C and 160 rpm for 24 hours. Blank suspension served as control. It is noteworthy that the samples had been autoclaved for sterilization before incubation. The samples from flasks were serially diluted in sterile physiological serum to prepare dilutions of  $10^{-1}$ ,  $10^{-2}$ ,  $10^{-3}$ ,  $10^{-4}$ , and  $10^{-5}$ . From each dilution, 10 and 100 microliters were transferred to petri dishes with solid culture medium to determine the optimal dilution for colony counting. Each sample was repeated three times, and the plates were incubated at 37°C for 48 hours. The number of colonies formed was counted, and the percentage of antibacterial activity was calculated using the Eq (1) [23].

$$R = (B-A)/B \times 100 \quad (1)$$

Where R is the inhibition rate, A is the number of colonies counted in the sample, and B is the number of bacteria counted in the control sample.

### 2.6. Cytotoxicity

The assessment of the samples' potential toxicity was carried out through the utilization of dimethylthiazol-2 and 5-diphenyltetrazolium bromide

(MTT) methodology on a mouse fibroblast cell lineage known as L-929. In this method, the viability of cells was assessed to determine the compatibility of the desired product. For each substance, the cell viability was determined by the formation of formazan color through the reduction of the compound MTT or other tetrazolium salts. Mitochondrial enzymes in living cells cleaved the tetrazolium ring, resulting in the formation of soluble purple formazan crystals. The presence of these crystals indicates the activity of limited enzymes and the quality of cell survival in the test sample. Finally, the percentage of surviving cells could be determined by measuring the absorbance at a wavelength of 570 nm using the ELISA reader (Model: ELx808, BioTek, USA).

### 2.7. Bioactivity

The osteogenic potential of the nanocomposite coatings was evaluated through immersion in Simulated Body Fluid (SBF) using Kokubo's method [24] for 28 days at 36.5°C according to ISO 23317 standard [25]. Over 28 days, throughout this period, the pH of the SBF solution was checked every 48 hours, and then the solution was replaced with a fresh solution, which was added to the Falcon for all samples. Each sample required 10 cm<sup>3</sup> of solution, determined by the formula Eq. (2):

$$SA/V = 0.1 \text{ cm}^{-1} \quad (2)$$

Where SA represents the sample's surface area in cm<sup>2</sup> and V is the necessary solution volume in cm<sup>3</sup>. Afterward, the samples were rinsed with distilled water and dried at ambient temperature or lab environment.

## 3. RESULTS AND DISCUSSION

### 3.1. Microstructural Analysis of the Precursor and Nanocomposite Films

The X-ray diffraction spectra for nanocomposite film containing CuO with different morphologies are displayed in Fig. 3. Detailed information regarding the compound name, chemical formula, and reference card number for each phase can be found in Table 2. As can be seen, the peaks of pure materials (CuO and Al<sub>2</sub>O<sub>3</sub>) are detectable for films with nanoplate CuO, but for films with spherical CuO, copper oxide (CuO) was reduced to Cu<sub>2</sub>O, because of the instability of sol-gel nanoparticles at high temperature (The purchased CuO nanosphere is made by the sol-gel method).

Films containing CuO nanoplate were synthesized by hydrothermal more stability is observed [26, 27].

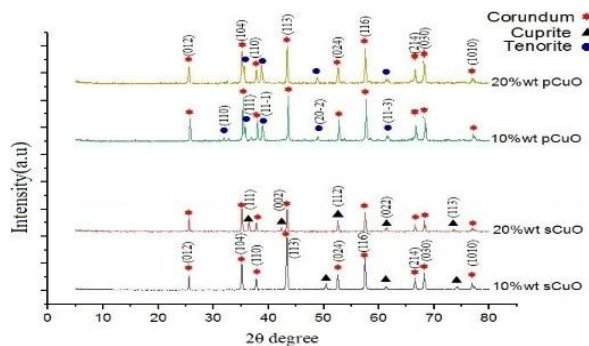


**Fig. 3.** XRD pattern of SPS nanocomposite

**Table 2.** The names of the compounds, their chemical formulas, and reference card numbers for the phases shown in Fig. 3

Chemical formula	Compound name	Reference card number
$\alpha\text{-Al}_2\text{O}_3$	Alpha-Alumina (Corundum)	96-900-9683
CuO	Tenorite	96-101-1149
$\text{Cu}_2\text{O}$	Cuperite	96-900-7498

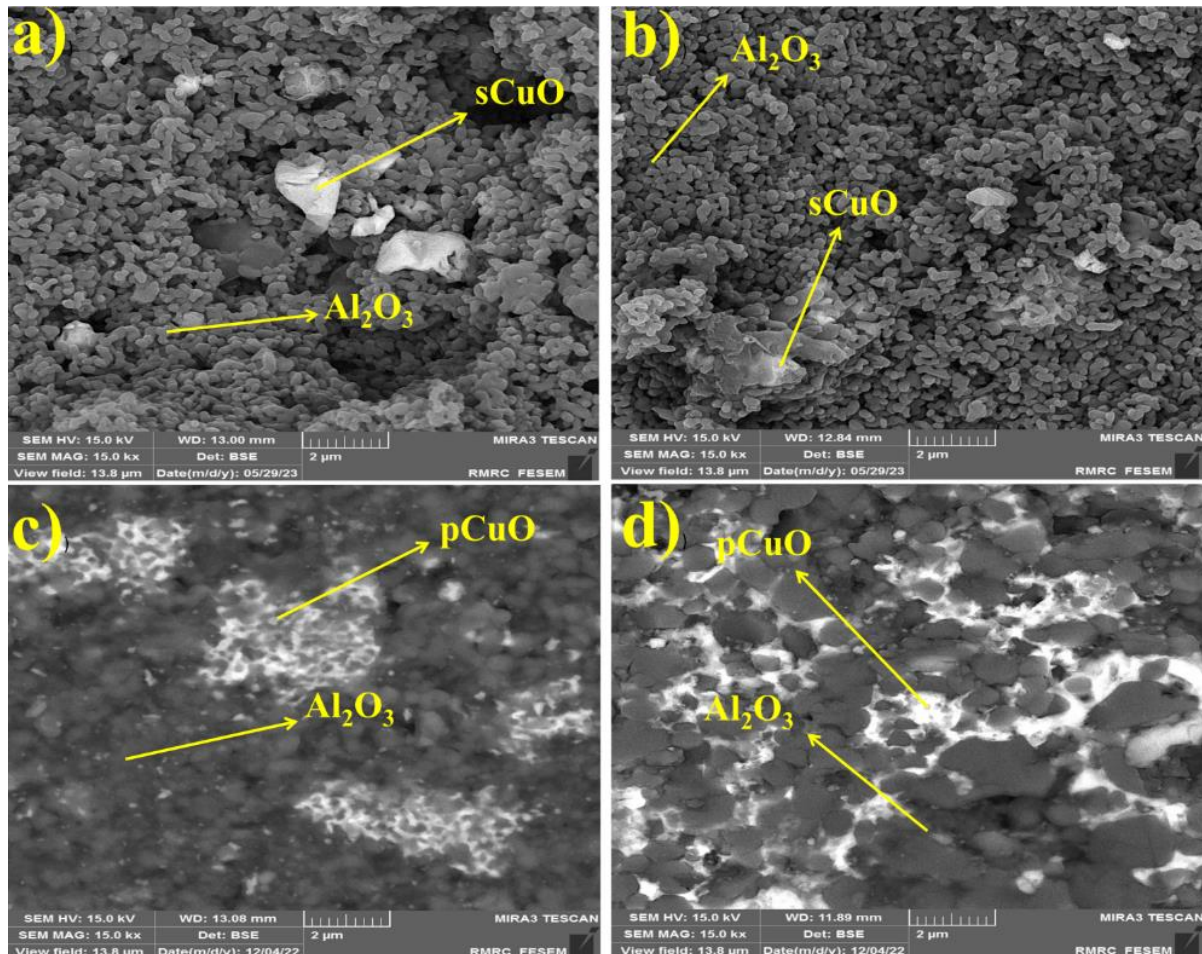


**Fig. 4.** FESEM images of nanocomposite films containing: a) 10% wt sCuO, b) 20% wt sCuO, c) 10% wt pCuO, d) 20% wt pCuO

Fig. 4 shows FESEM image of spark plasma sintered 10%wt sCuO, 20%wt sCuO, 10%wt pCuO, and 20%wt pCuO. There are three areas: 1) dark grey, 2) light white, and 3) the dark area. The light white areas indicate the presence of the copper oxide phase, while the dark gray areas are associated with the alumina phase. The dark areas in the images suggest the existence of porosity. Unlike conventional sintering techniques that often degrade nanoparticle morphology, SPS preserved the unique shapes of spherical (sCuO) and nanoplate (pCuO) CuO structures. This preservation was crucial for showcasing morphology-dependent antibacterial and bioactivity outcomes.

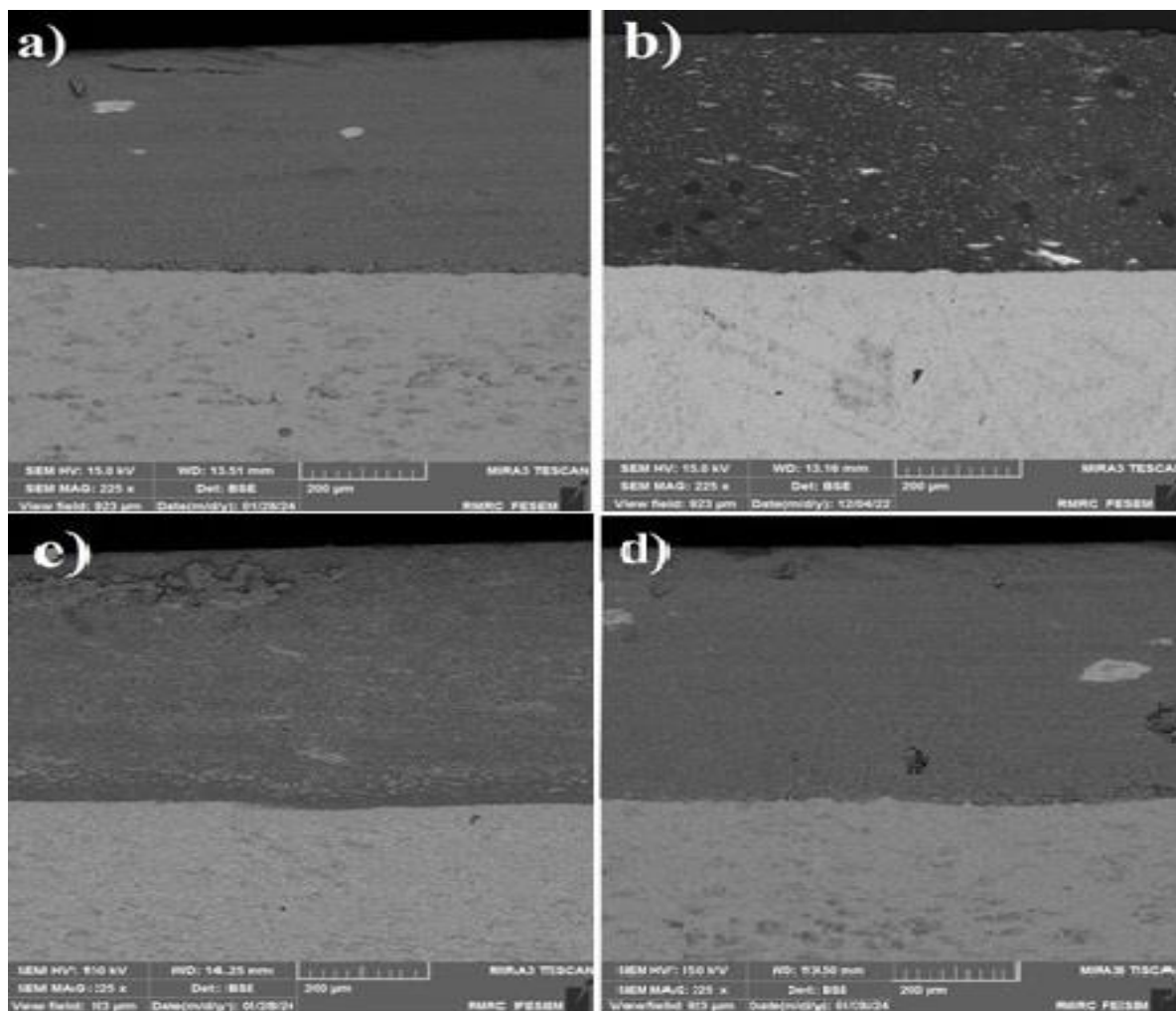
The high-pressure environment and rapid heating of SPS enabled strong adhesion of the nanocomposite coatings to titanium substrates, as evidenced by FESEM cross-sectional analyses. The absence of cracks and uniform coating thickness ( $\sim 260 \pm 20 \mu\text{m}$ ) underscores the method's reliability for biomedical applications. Fig. 5 shows cross-section FESEM images of the sample.

Fig. 6 shows a map analysis of cross-section films (20%wt pCuO, 20%wt sCuO), which indicates the distribution of elements in the entire coating created has almost the same distribution of elements, showing that the powder mixed by the high-energy ball mill is well mixed and has a uniform distribution, and no agglomeration and inhomogeneity can be seen. Fig. 7 illustrates the result of Energy Dispersive X-Ray (EDS) Analysis. The results confirm the presence of copper, aluminum, and oxygen elements. Additionally, it

indicates a nanocomposite film containing spherical copper oxide that lost oxygen during coating, which was confirmed by our XPS results.

XPS analysis was employed to examine the elemental surface chemical composition of a 20%wt sCuO and pCuO nanocomposite. The XPS spectra for the nanocomposites are shown in Fig. 8. Based on the survey spectrum of 20% wt sCuO and 20% wt pCuO (Fig. 8a), the peaks of Al (2p), Cu (2p), and O (1s) suggest the existence of copper oxide, carbon, aluminum oxide, and oxygen elements in the nanocomposite, respectively. There is no peak corresponding to impurity elements in the XPS spectrum.

The Al (2p) window is displayed in Fig. 8b; the main peak is at 74.8 eV and can be deconvoluted by a doublet peak (Al 2p<sub>3/2</sub>: 74.2 eV, Al 2p<sub>1/2</sub>: 75.3 eV), indicating the existence of O-Al-O bonds [23, 24].



**Fig. 5.** FESEM images of cross-section films containing: a) 10%wt sCuO, b) 20%wt sCuO, c) 10%wt pCuO, and d) 20%wt pCuO

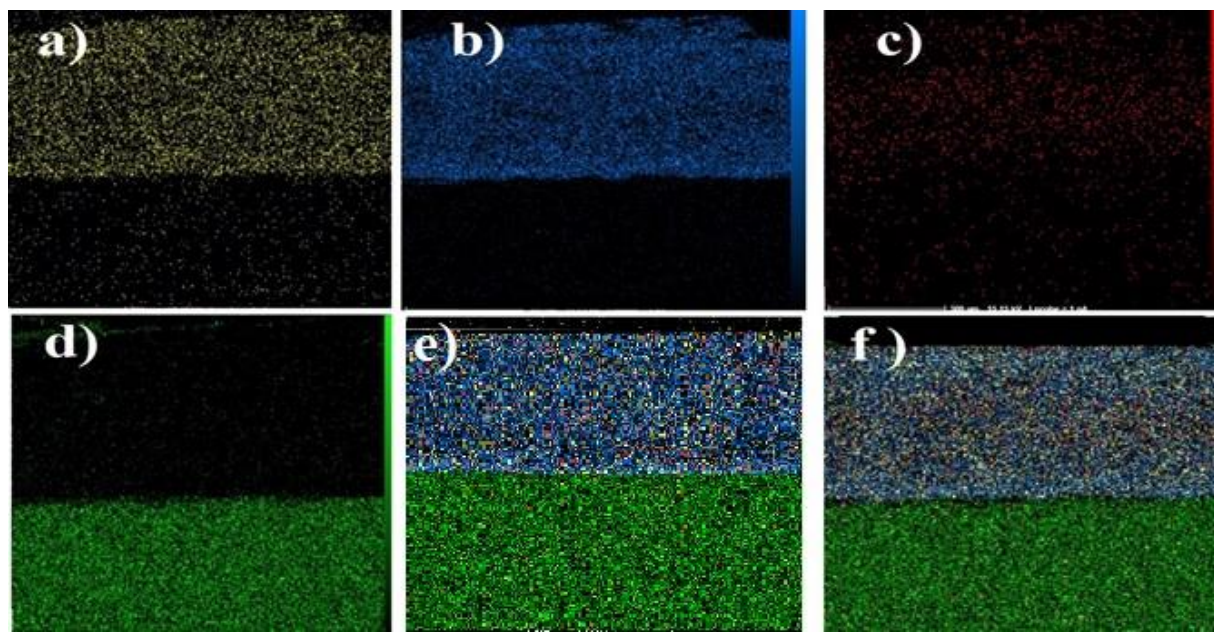


**Fig. 6.** Map analysis of cross-section films: a) Oxygen, b) Aluminum, c) Copper, d) Titanium, e) 20%wt sCuO, and f) 20%wt pCuO

Representation of O (1s) showing the peak position of O<sup>2-</sup> phase at  $530.08 \pm 0.1$  eV and the 1s peak of oxygen vacancy (V<sup>0</sup>)/adsorbed O<sup>0</sup> phase at  $531.49 \pm 0.1$  eV. A peak at E= 1.3-1.4 eV, higher in energy than the main O<sub>1s</sub> (532.98) peak (Fig. 8c), is assigned to the Al-OH species. The existence of these species aligns with the Trimethylaluminium (TMA) and H<sub>2</sub>O chemistry. Deconvoluted XPS spectra of Cu 2p<sub>3/2</sub> and Cu 2p<sub>1/2</sub> peaks appear in Fig. 8(d,e).

The XPS peak fitting revealed the Cu2p<sub>3/2</sub> peak displaying notable emissions of Cu<sup>2+</sup> at

$933.80 \pm 0.1$  eV and Cu<sup>+</sup> at  $935.30 \pm 0.1$  and  $934.65$  eV, indicating the presence of Cu<sup>+</sup> in the 934.65 peak of the pCuO sample (Fig. 6d), associated with Cu-O bonding. In Fig. 6e, the sCuO sample window is depicted, with the main peak showing two distinct peaks: 935.30 related to Cu<sup>+</sup> and Cu-O bonding, also 933.80 related to Cu<sup>2+</sup> and Cu<sub>2</sub>O bonding. Based on XPS results, the copper oxide structure (sCuO) wasn't fully converted to Cu<sub>2</sub>O during coating. The weight percentages of CuO and Cu<sub>2</sub>O on the surface are 64.7 and 35.3, respectively.

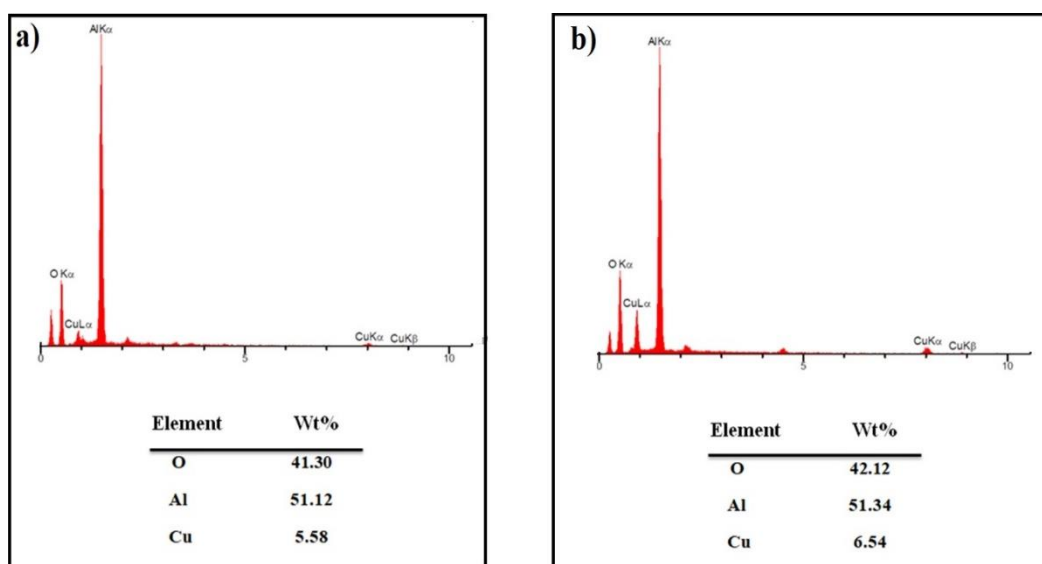


**Fig. 7.** EDS of film a) 20%wt pCuO, and b) 20%wt sCuO

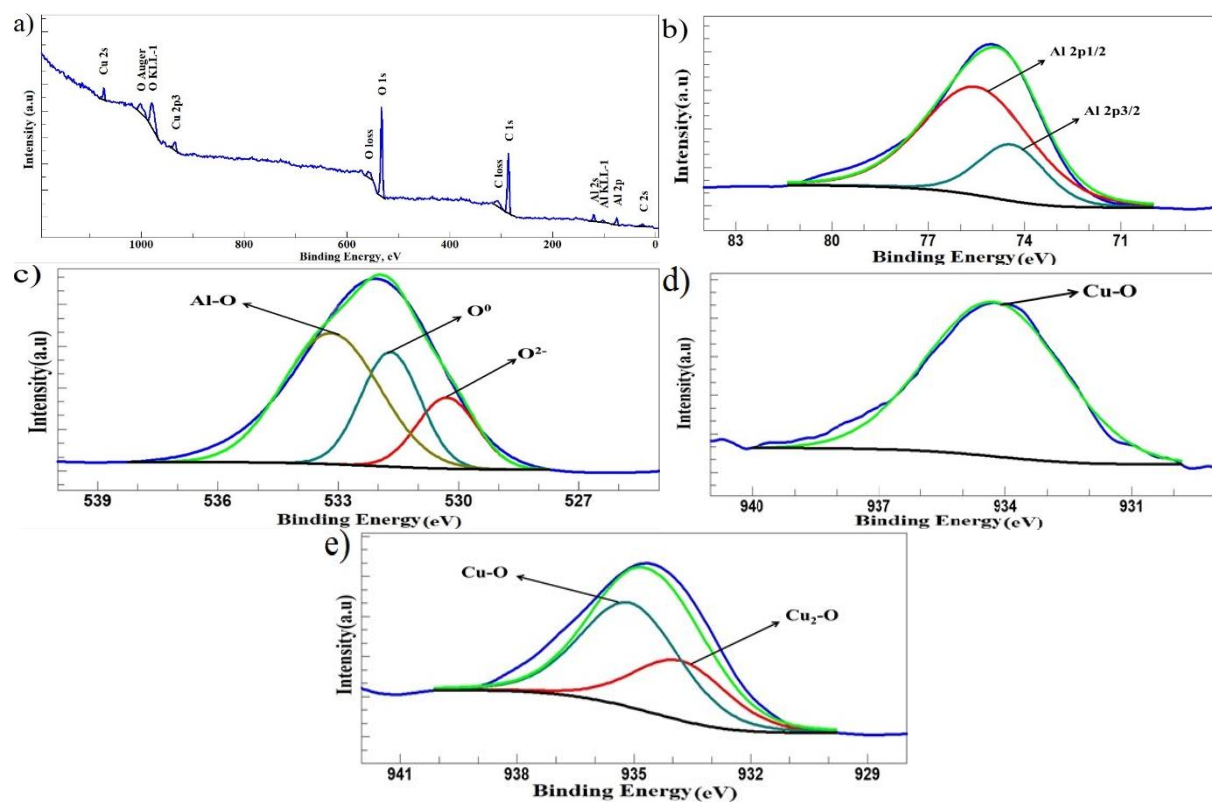


**Fig. 8.** a) XPS survey spectrum of the nanocomposite; high-resolution core-level XPS windows spectra of: b) Al (2p), c) O (1s), d) Cu (2p) for pCuO, and e) Cu (2p) for sCuO

The distinction between XRD and XPS interpretations is due to their varying experimental mechanisms [36, 37]. The FTIR results showed that both pCuONP and sCuONP spectra had multiple peaks of functional groups (Fig. 9).

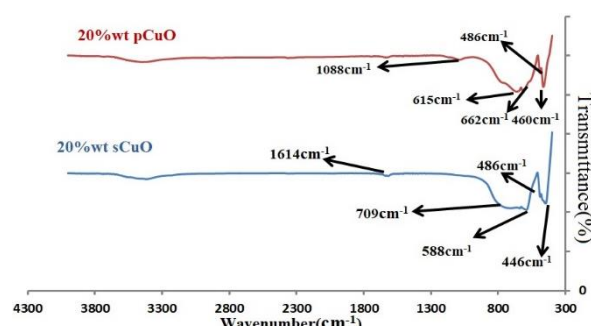


**Fig. 9.** FTIR spectra of 20%wt pCuO NP and 20%wt sCuO NP

The observed peaks indicated at 1088 cm<sup>-1</sup> are associated with CO stretching, and 1614 cm<sup>-1</sup> corresponds to the stretching and bending vibrations of O-H in absorbed water. The characteristic peaks at 615 cm<sup>-1</sup> and 588 cm<sup>-1</sup> are attributed to the formation of CuO/Al<sub>2</sub>O<sub>3</sub> nanocomposite. The bands observed at 662 cm<sup>-1</sup> and 709 cm<sup>-1</sup>

corresponded to the stretching vibration of the Al-O bond. Finally, the absorption peaks positioned from 446 cm<sup>-1</sup> to 588 cm<sup>-1</sup> region revealed the presence of characteristic peaks of Cu-O.

### 3.2. Antibacterial Activity

Antibacterial activities of the synthesized nanocomposite against *E.coli* and *S.aureus* bacteria (for 12 h at 37°C) were investigated using the colony-counting method (Eq. (1)). Fig. 10(a,b) illustrates images of agar and a control sample containing no antibacterial agent in the *E.coli* and *S. aureus* culture medium. At first, the antibacterial activity of the base metal (titanium) was investigated. Generally, pure Titanium metal itself does not have significant antibacterial properties. Wei Jiang [28], while researching Al<sub>2</sub>O<sub>3</sub> nanoparticles, exhibited mortality rates of 57% for *Bacillus subtilis* (*B. subtilis*), 36% for *E. coli*, and 70% for *Pseudomonas fluorescens* (*P. fluorescens*). Based on Fig. 11, it can be seen that the incorporation of nano copper oxide and alumina effectively increases the antibacterial property, which leads to synergistic effects of the combination of copper oxide with alumina. The remarkable antibacterial activity of pCuO

samples was previously reported to be due to an increase in surface area, which increased bacterial interactions [29]. According to our results (Fig. 11) and previous studies the antibacterial effect of CuO-NPs depends not only on their morphology and size, but also on the type of microorganism, *S. aureus* showed greater resistance to CuO-NP, while *E. coli* was more susceptible to them [30]. Luz E.Roman [31] believed that CuO nanoparticles bound to the bacterial cell wall dissolve, and CuO<sup>2+</sup> ions are transferred into the cytoplasmic membrane. The layer on the outer membrane of *E. coli* bacteria whose name is Lipoteichoic acid, contains large amounts of negatively charged

lipopolysaccharides that may supply attachment parts for CuO nanoparticles. However, studies are required to make clear the mechanisms behind these morphological effects.

### 3.3. Cytotoxicity Test

The effect of all samples on cell viability was obtained according to the following relationship:  $\text{Viability} = \text{OD}_C / \text{OD}_R$  (3) The optical density of films and control samples is represented by ODC and ODR, respectively. The cell viability percentage of s-CuO NP (10, 20%wt) and p-CuO NP (10, 20%wt) films is presented in Table 3 and Fig. 12.

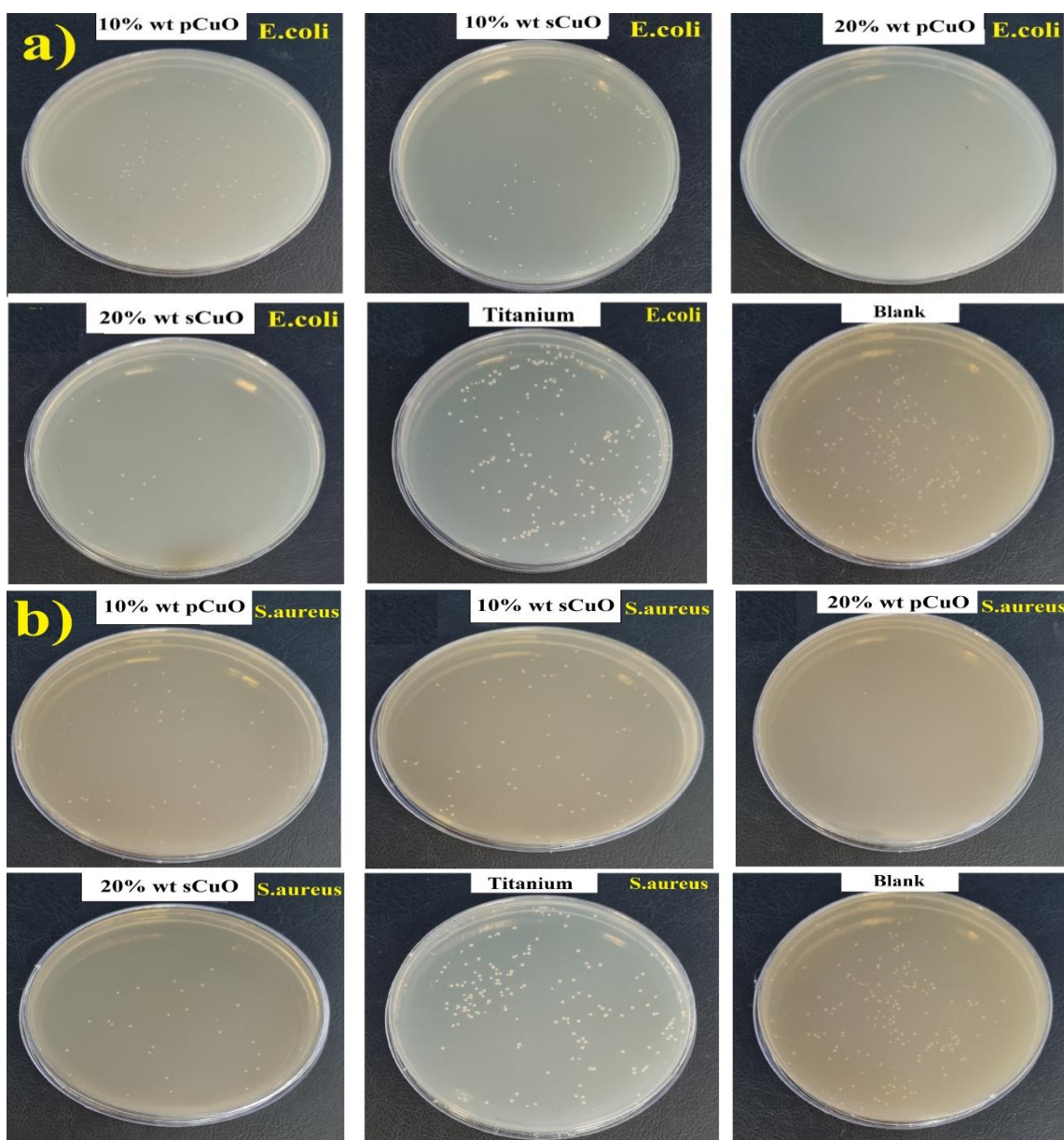


**Fig. 10.** Antibacterial test images of agar: a) *E. coli*, b) *S. aureus*, and Blank after 12 h of contact with *E. coli* at 37°C

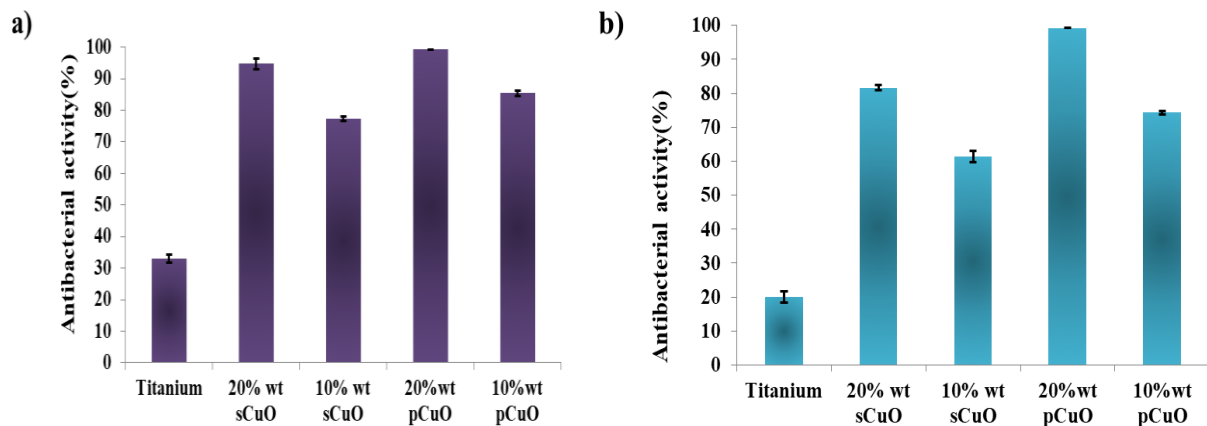


**Fig. 11.** The antibacterial activity test after 12 h of contact with a) *E. coli* and b) *S. aureus* at 37°C

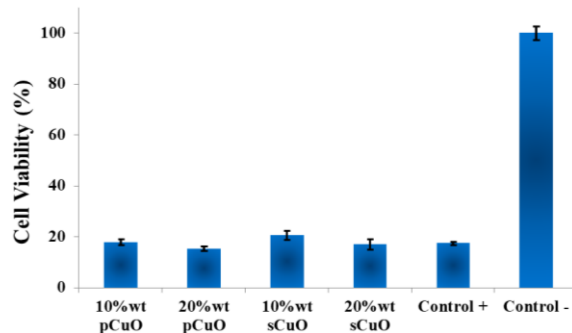


**Fig. 12.** The Cells viability percentage comparison of nanocomposites

Normally,  $\text{Al}_2\text{O}_3$  nanoparticles exhibited non-toxic impact at the concentration of 500  $\mu\text{g}/\text{mL}$  and lower, thus cytotoxicity was influenced by concentration, exposure time, and cell type [32]. It has been shown in various studies that the direct contact of nano copper oxide with cells leads to cell death. Also, Luz E [31] determined during research that the use of nano copper oxide particles in the equipment and clothes of health centers can improve health, and help to remove Healthcare-Associated Infections (HAIs), and it is non-toxic to human skin, because it does not have direct contact with our cells. Hossein Alishah [33] reported the effect of nano copper oxide during the MTT assay on cancer cells (MCF-7), which indicated the highest anti-cancer activity at a concentration of 160  $\mu\text{g}/\text{ml}$ ; therefore, like our

results, cell viability decreased as the concentration of copper oxide nanoparticles increased (dose-dependent). According to the results obtained, it can be understood that sCuO-NP is less toxic than pCuO-NP. Nanoplate copper oxide, due to its high surface reactivity, exhibited greater toxicity compared to spherical nanoparticles. Generally, previous studies reported of mechanisms of nano-copper oxide effect on cells and their interactions with each other, but the main finding was that  $\text{Cu}^{2+}$  release from CuO NPs caused toxic effects by generating ROS and damaging cellular DNA [34].

### 3.4. Bioactivity Test

Based on our results, 20% wt sCuO and pCuO exhibited higher antibacterial activity compared to the other samples. Therefore, it was selected as the optimum nanocomposite, and a bioactivity assay was carried out on it. The ramps between each time point showed the increase in pH due to the release of ions from the nanocomposites into the solution. The pH drop noted every 48 hours resulted from the complete solution replacement, simulating fluid recirculation under physiological conditions. No pH-related toxicity issues were predicted since the maximum pH reached during soaking was approximately 7.7 for both samples (Fig. 13). This slight increase in pH may even enhance osteoblast activity, which is often boosted in a mildly alkaline environment.

**Table 3.** Cell viability percentage of control, 10%, and 20% pCuO and sCuO

Sampsels	Average OD	Average control	Viability (%)
10%wt pCuO	0.084	0.470666667	17.91785
20%wt pCuO	0.072	0.470666667	15.36827
10%wt sCuO	0.097	0.470666667	20.60907
20%wt sCuO	0.080	0.470666667	17.06799
Control +	0.082	0.470666667	17.4221
Control -	0.470	0.470666667	100

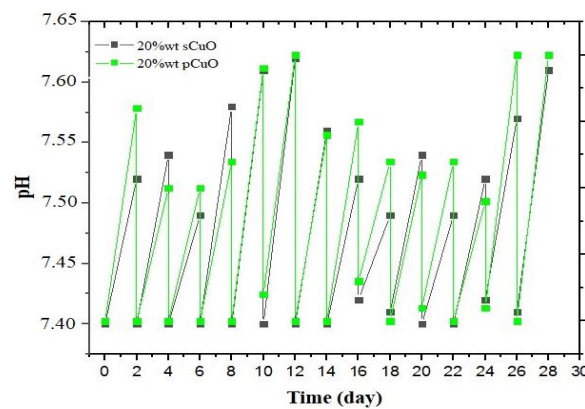


**Fig. 13.** pH variation over immersion time in SBF

In vitro bioactivity experiment in SBF indicated that the nanofilms effectively form Hydroxyapatite (HA). After 14 days of immersion, the surface appears to be covered by a thin layer of HA; Surface changes were evident (Fig. 14a,b). After 28 days, the surface of both samples appeared to be completely covered by a homogeneous layer of HA (Fig. 14c,d). The formation of an HA layer on biomaterial surfaces is critical for interfacial bonding with bone post-implantation, as osteoblasts adhere to and proliferate on this calcium-phosphate layer, facilitating new bone production [49]. Semi-quantitative EDS analyses of the nanofilms' surfaces after soaking in SBF for 14 and 28 days submitted Ca/P molar ratios of  $1.61 \pm 0.04$  and  $1.59 \pm 0.05$

(calculated on three sites) for 20%wt pCuO and sCuO samples, respectively. These values are near the stoichiometric HA (1.67), indicating an advanced stage of the sample surface's conversion to HA. EDS analysis revealed that the Al and Cu peak decrease after 14 days immersion in SBF (Fig. 14.e,f), while the peaks of Ca and P are clearly visible after 28 days (Fig. 14.g). This indicates that the nanofilm surface was fully covered by a thick layer of calcium phosphate. As additional evidence of the good HA-forming ability of the nanofilm, XRD analyses were carried out on 20%wt sCuO and 20%wt pCuO samples immersed up to 28 days in SBF (Fig. 15). The analysis showed that the diffraction peaks indicating the HA crystalline phase were almost visible after 28 days of immersion in SBF. A major peak was observed at approximately  $32^\circ$  (211), indicating the main reflection of HA. Additionally, the other major HA peak emerged at  $26.2^\circ$  (002), corresponding to the reflection of HA. In comparison of two different morphologies of copper oxide and based on the number of peaks in X-ray analysis (Fig. 15), it can be inferred that the quantity of apatite formed in the nanoplate structure exceeds that of its spherical shape. Therefore, the formation of hydroxyapatite (HA) layers was observed, demonstrating the material's ability to support bone regeneration.

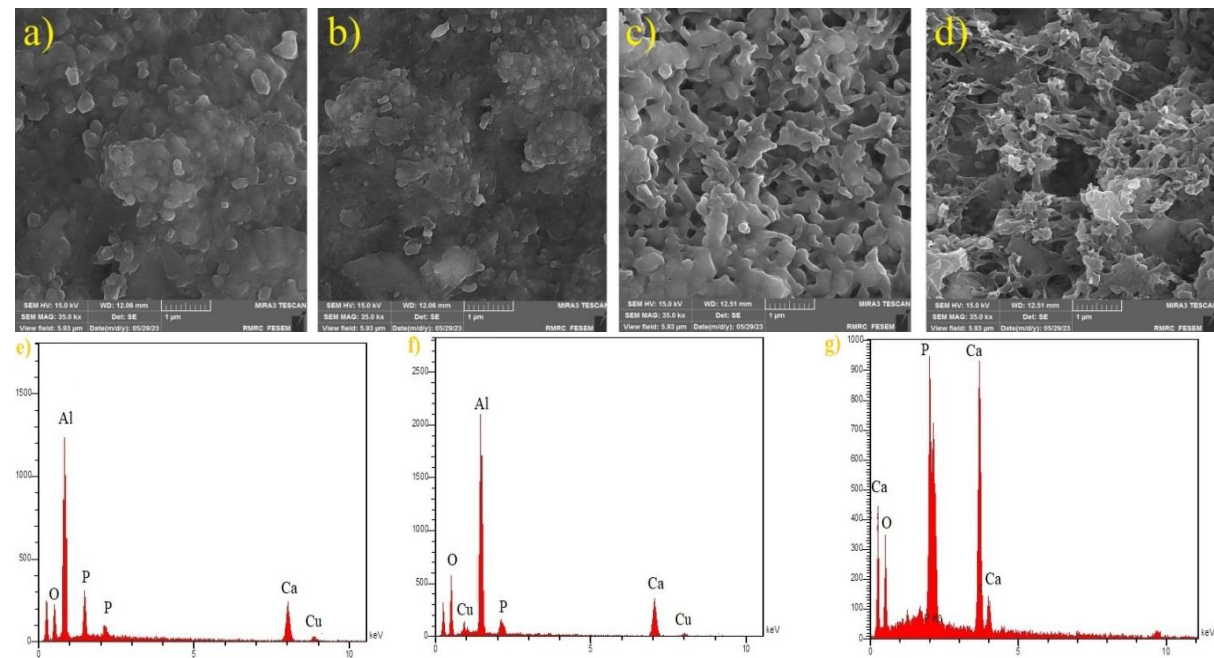


**Fig. 14.** FESEM micrographs of the surface of 20%wt sCuO (a, c) and 20%wt pCuO (b, d) nanofilms after immersion in SBF for 14 and 28 days; EDS spectrum of the newly formed surface layer on both sample after 14 and 28 days in SBF (e, f, g)

Nanoplates exhibited superior HA formation compared to spherical CuO, as confirmed by XRD and EDS analyses, with prominent peaks indicating well-crystallized HA.

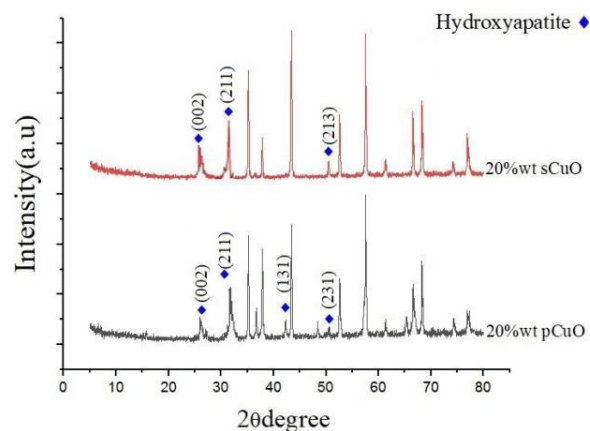


**Fig. 15.** XRD pattern of nanocomposite after 28 days immersed in SBF solution

**Table 4.** Compounds, chemical formulas, and reference card numbers for the phases shown in Fig. 14

Chemical formula	Compound name	Reference card number
Ca <sub>5</sub> (PO <sub>4</sub> ) <sub>3</sub> OH	Hydroxyapatite	96-101-1243

#### 4. CONCLUSIONS

Orthopedic implants face the dual challenge of preventing postoperative infections while promoting osseointegration for long-term stability. To address these issues, we have developed nanocomposite coatings of CuO/Al<sub>2</sub>O<sub>3</sub> with distinct CuO morphologies (spherical and nanoplate), deposited on titanium substrates using the Spark Plasma Sintering (SPS) method. This innovative coating exhibits antimicrobial efficacy against *E. coli* and *S. aureus* while simultaneously fostering osteogenic activity, as evidenced by MTT and SBF assays. XRD, FTIR, and XPS analyses exhibited the successful synthesis of the nanocomposites. The combination of Copper oxide and Alumina demonstrated strong antibacterial properties, effectively inhibiting the growth of *S. aureus* and *E. coli*, with nanoplate Copper oxide proving more effective than its spherical counterpart. MTT results indicate that cell viability decreases as copper oxide concentration increases (dose dependent). Conversely, two nanocomposites containing 20% by weight of copper oxide with different morphologies passed the biocompatibility test.

#### ACKNOWLEDGMENT

The authors would like to thank the Materials and Energy Research Center for financial support of this student project (Grant No. 771401055).

#### REFERENCES

- [1] Fatemeh Sajedi Alvar, Mojgan Heydari, Asghar Kazemzadeh, Mohammad Reza Vaezi, Leila Nikzad. "Synthesis and characterization of corrosion-resistant and biocompatible Al<sub>2</sub>O<sub>3</sub>–TiB<sub>2</sub> nanocomposite films on pure titanium". Ceramics International 46 (2020) 4215–4221. DOI: 10.1016/j.ceramint.2019.10.140.
- [2] Yuan Zhang, Shan Fu, Lei Yang, Gaowu Qin, Erlin Zhang. "A nano-structured TiO<sub>2</sub>/CuO/Cu<sub>2</sub>O coating on Ti-Cu alloy with dual function of antibacterial ability and osteogenic activity". Journal of Materials Science & Technology 97 (2022) 201–212. DOI: 10.1016/j.jmst.2021.04.056.
- [3] Richard Bright, Daniel Fernandes, Jonathan Wood, Dennis Palms, Anouck Burzava, Neethu Ninan, Toby Brown, Dan Barker, Krasimir Vasilev. "Long-term antibacterial properties of a nanostructured titanium alloy surface: An in vitro study". Materials Today Bio 13 (2021) 100176-89. DOI: 10.1016/j.mtbiol.2021.100176.
- [4] Chouirfa H, Bouloussa H, Migonney V, Falentin-Daudré C. "Review of titanium surface modification techniques and coatings for antibacterial applications". Acta Biomater (2019) 37-54. DOI: 10.1016/j.actbio.2018.10.036.
- [5] Amal M. Al-Mohaimeed, Gamal A. E. Mostafa, and Maha F. El-Tohamy. "New Construction of Functionalized CuO/Al<sub>2</sub>O<sub>3</sub> Nanocomposite-Based Polymeric Sensor for Potentiometric Estimation of Naltrexone Hydrochloride in Commercial Formulations". Polymers (Basel) 13 (2021) 4459-78. DOI: 10.3390/polym13244459.
- [6] Md. Jasim Uddin, Mst. Sarmina Yeasmin, Ali Ahsan Muzahid, Md. Mahmudur Rahman, G.M. Masud Rana, Tahmina Akter Chowdhury, Md. Al-Amin, Md. Kazi Wakib, Sayeda Halima Begum. "Morphostructural studies of pure and mixed metal oxide nanoparticles of Cu with

Ni and Zn". *Heliyon* 10, (2024). e 30544. DOI: 10.1016/j.heliyon.2024.e30544.

[7] Mohsin Ali, Muhammad Ijaz, Muhammad Ikram, Anwar Ul-Hamid, Muhammad Avais & Aftab Ahmad Anjum. "Biogenic Synthesis, Characterization and Antibacterial Potential Evaluation of Copper Oxide Nanoparticles against *Escherichia coli*". *Nanoscale Res. Lett* 16 (2021), 148-161. DOI: 10.1186/s11671-021-03605-z.

[8] Sergey V. Gudkov, Dmitriy E. Burmistrov, Veronika. Smirnova, Anastasia. Semenov and Andrey B. Lisitsyn. "A Mini Review of Antibacterial Properties of  $\text{Al}_2\text{O}_3$  Nanoparticles" *Nanomaterials* (Basel) 12 (2022), 2635-52. DOI: 10.3390/nano12152635.

[9] Xia, T; Kovochich, M.; Brant, J.; Hotze, M.; Sempf, J.; Oberley, T.; Sioutas, C.; Yeh, J.I.; Wiesner, M.R.; Nel, A.E. "Comparison of the abilities of ambient and manufactured nanoparticles to induce cellular toxicity according to an oxidative stress paradigm". *Nano Lett.* (2006) 1794–1807. DOI: 10.1021/nl061025k.

[10] Paolo Zatta, Tamas Kiss, Mario Suwalsky, Guy Berthon. "Aluminium (III) as a promoter of cellular oxidation". *Coordination Chemistry Reviews* 228 (2002), 271-284. DOI: 10.1016/S0010-8545(02)00074-7.

[11] Pakrashi, S; Dalai, S; Ritika; Sneha, B.; Chandrasekaran, N.; Mukherjee, A. "A temporal study on fate of  $\text{Al}_2\text{O}_3$  nanoparticles in a fresh water microcosm at environmentally relevant low concentrations". *Ecotoxicology and Environmental Safety* 84. (2012), 70–77. DOI: 10.1016/j.ecoenv.2012.06.015.

[12] Arul Prakash F., G. J. Dushendra Babu, M. Lavanya, K. Shenbaga Vidhya and T. Devasena. "Toxicity Studies of Aluminium Oxide Nanoparticles in Cell Lines". *International Journal of Nanotechnology and Applications* 5, (2011). 99-107. DOI: 10.1016/j.ecoenv.2011.06. 25.

[13] M.U. Anu Prathap, Balwinder Kaur, Rajendra Srivastava. "Hydrothermal synthesis of  $\text{CuO}$  micro-/nanostructures and their applications in the oxidative degradation of methylene blue and non-enzymatic sensing of glucose/ $\text{H}_2\text{O}_2$ ". *Journal of Colloid and Interface Science* 370 (2012) 144–154. DOI:10.1016/j.jcis.2011.12.074.

[14] Seyed Javad Davarpanah, Ramin Karimian, Vahabodin Goodarzi, Farideh Piri. "Synthesis of Copper (II) Oxide ( $\text{CuO}$ ) Nanoparticles and Its Application as Gas Sensor". *Journal of Applied Biotechnology Reports* 2, (2015). 329-332. DOI10.1021/3c01155.

[15] Yuanyuan Ma, Hui Wang, Julian Key b, Shan Ji, Weizhong Lv, Rongfang Wang. "Control of  $\text{CuO}$  nanocrystal morphology from ultrathin "willow-leaf" to "flower-shaped" for increased hydrazine oxidation activity". *Journal of Power Sources* 300 (2015) 344e350. DOI: 10.1016/j.jpowsour.2015.09.087.

[16] Mojtaba Taran, Maryam Rad, Mehran Alavi. "Antibacterial Activity of Copper Oxide ( $\text{CuO}$ ) Nanoparticles Biosynthesized by *Bacillus sp*". *Optimization of Experiment Design*. 23 (2017) 198-206. DOI: 10.15171/PS.2017.30.

[17] K. J. Arun1, A. K. Batra. Krishna, K. Bhat, M. D. Aggarwal, J. P. Francis. "Surfactant Free Hydrothermal Synthesis of Copper Oxide Nanoparticles". *American Journal of Materials Science* 5 2015, 36-38. DOI: 10.5923/s.materials.201502.06.

[18] Surapaneni Meghana, Prachi Kabra, Swati Chakraborty and Nagarajan Padmavathy. "Understanding the pathway of antibacterial activity of copper oxide nanoparticles". *RSC Adv* 5, (2015), 12293-12299. DOI: 10.1039/c4ra12163e.

[19] Shima Tavakoli, Mahshid Kharaziha, Shokouh Ahmadi. Green Synthesis and Morphology Dependent Antibacterial Activity of Copper Oxide Nanoparticles. *J Nanostruct* 9(1) (2019)163-171. DOI: 10.22052/JNS.2019.01.018.

[20] Mohammad Abedi, Atefeh Asadi, Stepan Vorotilo, and Alexander S. Mukasyan. "A critical review on spark plasma sintering of copper band its alloys". *Journal of Materials Science* 56 (2021) 19739–19766. DOI: 10.1007/s10853-021-06556-z.

[21] Nouari Saheb, Zafar Iqbal, Abdullah Khalil, Abbas Saeed Hakeem, Nasser Al Aqeeli, Tahar Laoui, Amro Al-Qutub, and René Kirchner. "Park Plasma Sintering of Metals and Metal MatrixNanocomposites: A Review". *Journal of Nanomaterials* 13, (2012), 983470-83, DOI: 10.1155/2012/983470.

[22] Christophe Tenailleau, Guillaume Salek,

Thi Ly Le, Benjamin Dupoyer, Jean-Jacques Demai, Pascal Dufour & Sophie Guillemet-Fritsch. "Heterojunction p-Cu<sub>2</sub>O/ZnO-n solar cell fabricated by spark plasma sintering". *Materials for Renewable and Sustainable Energy* 6, (2017) 6-18. DOI: 10.1007/s40243-017-0102-8.

[23] Reza Ahmadi, Raziye Fattahi Nafchi, Parvaneh Sangpour, Mozhgan Bagheri, Tohid Rahimi. "Evaluation of antibacterial behavior of in situ grown CuO-GO nanocomposites". *Materials Today Commun* 28 (2021), 102642, DOI: 10.1016/J.MTCOMM.2021.102642.

[24] Tadashi Kokubo, Hiroaki Takadama. "How useful is SBF in predicting in vivo bone bioactivity?". *Biomaterials* 27 (15) (2006) 2907–2915, DOI: 10.1016/j.biomaterials.2006.01.017.

[25] International Organization for Standardization. (2007). *Implants for surgery—In vitro evaluation for apatite-forming ability of implant materials*. ISO/CDIS 23317. <https://www.iso.org/standard/65054.html>.

[26] Martina Kocjan and Matejka Podlogar. Perspective Chapter: "Modification Engineering of Titanium Dioxide-Based Nanostructured Photocatalysts for Efficient Removal of Pollutants from Water". *Titanium Dioxide -Uses, Applications, and Advances* 23 (2024) 1-11. DOI: 10.5772/intechopen.1007375.

[27] Muhammad Hamzah Saleem, Ujala Ejaz, Meththika Vithanage, Nanthi Bolan & Kadambot H. M. Siddique. "Synthesis, characterization, and advanced sustainable applications of copper oxide nanoparticles: a review". *Clean Techn Environ Policy*. Mar 13 (2024). DOI: 10.1007/s10098-024-02774-6.

[28] Wei Jiang, Hamid Mashayekhi, Baoshan Xing. "Bacterial toxicity comparison between nano-and micro-scaled oxide particles". *Environmental Pollution* 157 (2009) 1619–25. DOI: 10.1016/j.envpol.2008.12.025.

[29] Lu Xiong, Zhong-Hua Tong, Jie-Jie Chen, Ling-Li Li, Han-Qing Yu. "Morphology-dependent antimicrobial activity of Cu/Cu<sub>x</sub>O nanoparticles". *Ecotoxicology* 24 (2015). 2067-72. DOI: 10.1007/s10646-015-1554-1.

[30] Sharma P, Goyal D, Chudasama B. "Antibacterial activity of colloidal copper nanoparticles against Gram-negative (*Escherichia coli* and *Proteus vulgaris*) bacteria". *Lett Appl Microbiol* 74(5) (2022); 695-706. DOI: 10.1111/lam.13655.

[31] Luz E. Román, Enrique D. Gomez, José L. Solís and Mónica M. Gómez. "Antibacterial Cotton Fabric Functionalized with Copper Oxide Nanoparticles". *Molecules* 25 (2020), 5802; DOI: 10.3390/molecules25245802.

[32] Alhaji Modu Bukar, Faez Firdaus Abdullah Jesse, Che Azurahanim Che Abdullah, Mustapha M. Noordin, Modu Z. Kyari, Ashreen Norman & Mohd Azmi Mohd-Lila. "In vitro cytotoxicity evaluation of green synthesized alumina nanoscales on different mammalian cell lines". *Sci Rep* 14, 22826 (2024). DOI: 10.1038/s41598-024-53204-y.

[33] Hossein Alishah, Shahram Pourseyedi, S. Yousef Ebrahimipour, Saeed Esmaili Mahani3, Nahid Rafiei. "Green synthesis of starch-mediated CuO nanoparticles: preparation, characterization, antimicrobial activities and in vitro MTT assay against MCF-7 cell line". *Rend. Fis. Acc. Lincei* 28, (2017) 65–71. DOI: 10.1007/s12210-016-0574-y.

[34] Ya-Nan Chang, Mingyi Zhang, Lin Xia, Jun Zhang and Gengmei Xing. "The Toxic Effects and Mechanisms of CuO and ZnO Nanoparticles". *Materials* 5 (2012) 2850-2871. DOI: 10.3390/ma5122850.

[35] Nayak, B. B., Dash, T., & Mishra, B. K. "Purple Coloured Natural Ruby: X-ray Photoelectron Spectroscopy, X-ray Diffraction, X-ray Tomography and Other Microstructural Characterizations. International Journal of Sciences". *Basic and Applied Research (IJSBAR)* 25 (2016), 94–114.

[36] Anshuman Sahai, Navendu Goswami, S. D. Kaushik, Shilpa Tripathi. "Cu/Cu<sub>2</sub>O/CuO Nanoparticles: Novel Synthesis by Exploding Wire Technique and Extensive Characterization". *Applied Surface Science* 390 (2016), 974-983. DOI: 10.1016/j.apsusc.2016.09.005.

[37] T. Ghodselahi, M. A. Vesaghi, A. Shafeikhani, A. Baghizadeh, M. Lameii. "XPS study of the Cu@Cu<sub>2</sub>O core-shell nanoparticles". *Applied Surface Science*. 255 (2008), 2730-2734 DOI.org/10.1016/j.apsusc.2008.08.110.

[38] Muniratu Maliki, Ikhazuagbe H. Ifijen, Esther U. Ikuoria, Eribe M. Jonathan, Gregory E. Onaiwu, Ukeme D. Archibong & Augustine Ighodaro. "Copper nanoparticles and their oxides: optical, anticancer and antibacterial properties". International Nano Letters 12, (2022) 379-398. Doi.org/10.1007/s40089-022-00380-2.

[39] Kenneth Ssekatawa, Denis K. Byarugaba, Martin Kamilo Angwe, Eddie M. Wampande, Francis Ejobi, Edward Nxumalo, Malik Maaza, Juliet Sackey and John Baptist Kirabira. "Phyto-Mediated Copper Oxide Nanoparticles for Antibacterial, Antioxidant and Photocatalytic Performances". Front Bioeng Biotechnol 10 (2022) 16:10:820218. Doi.org/10.3389/fbioe.2022.820218.

[40] Evelyn Assadian, Mohammad Hadi Zarei, Ali Ghanadzadeh Gilani, Mehrzad Farshin, Hamid Degampanah & Jalal Pourahmad. "Toxicity of Copper Oxide (CuO) Nanoparticles on Human Blood Lymphocytes". Biol Trace Elem Res 184 (2018); 350-357 Doi.org/10.1007/s12011-017-1170-4.

[41] A. Muthuvel.M. Jothibas.C. Manoharan. "Synthesis of copper oxide nanoparticles by chemical and biogenic methods: photocatalytic degradation and in vitro antioxidant activity". Nanotechnology for Environmental Engineering 5, 14 (2020). Doi.org/10.1007/s41204-020-00078-w.

[42] Tiago José Marques Fraga, Caroline Maria Bezerra de Araújo, Maurício Alves da Motta Sobrinho, Marcos Gomes Ghislandi. "The role of multifunctional nanomaterials in the remediation of textile wastewaters". The Textile Institute Book Series 5 (2021), 95-136. Doi.org/10.1016/B978-0-323-85829-8.00001-8.

[43] Simbongile Sicwetsha. Sindisiwe Mvango. Tebello Nyokong. Philani Mashaz. "Effective ROS generation and morphological effect of copper oxide nanoparticles as catalysts". Journal of Nanoparticle Research 23 (2021): 227. DOI: 10.1007/s11051-021-05334-x.

[44] Surapaneni Meghana. Prachi Kabra. Swati Chakraborty band Nagarajan Padmavathy. "Understanding the pathway of antibacterial activity of copper oxide nanoparticles". RSC Adv5. (2015), 12293. Doi.org/10.1039/C4RA12163E.

[45] P.A. Prashantha, R.S. Raveendra, R. HariKrishnac, S. Anandad, N.P. Bhagya, B.M. Nagabhushanac, K. Lingaraju H. Raja Naika. "Synthesis, characterizations, antibacterial and photo luminescence studies of solution combustion derived  $\text{Al}_2\text{O}_3$  nanoparticles". Journal of Asian Ceramic Societies 3 (2015) 345–351. Doi.org/10.1016/j.jascer.2015.07.001

[46] Rajkumar Jana, Arka Dey, Mrinmay Das, Joydeep Datta, Pubali Das, Partha Pratim Ray. "Improving performance of device made up of CuO nanoparticles synthesized by hydrothermal over the reflux method". Applied Surface Science 452 (2018) 15, 155-164. Doi.org/10.1016/j.apsusc.2018.04.262.

[47] Sebastiano Di Buccianico, Maria Rita Fabbrizi, Superb K. Misra, Eugenia Valsami-Jones, Deborah Berhanu, Paul Reip, Enrico Bergamaschi and Lucia Migliore. "Multiple cytotoxic and genotoxic effects induced in vitro by differently shaped copper oxide nanomaterials". Mutagenesis 28 (2013); 28(3):287-99. Doi: 10.1093/mutage/get014.

[48] Elisa Fiume, Dilshat Tulyaganov, Graziano Ubertalli, Enrica Verné and Francesco Baino. "Dolomite-Foamed Bioactive Silicate Scaffolds for Bone Tissue Repair". Materials 13. (2020); 628-42. DOI:10.3390/ma13030628.